

OMPQ: Orthogonal Mixed Precision Quantization

Yuexiao Ma¹, Taisong Jin^{1*}, Xiawu Zheng¹, Yan Wang², Huixia Li¹,
Guannan Jiang³, Wei Zhang³, Rongrong Ji^{1,4}

¹School of Informatics, Xiamen University

²Pinterest, USA ³Contemporary Amperex Technology Co., Limited

⁴Institute of Artificial Intelligence, Xiamen University

Abstract

To bridge the ever increasing gap between deep neural networks' complexity and hardware capability, network quantization has attracted more and more research attention. The latest trend of mixed precision quantization takes advantage of hardware's multiple bit-width arithmetic operations to unleash the full potential of network quantization. However, this also results in a difficult integer programming formulation, and forces most existing approaches to use an extremely time-consuming search process even with various relaxations. Instead of solving a problem of the original integer programming, we propose to optimize a proxy metric, the concept of network orthogonality, which is highly correlated with the loss of the integer programming but also easy to optimize with linear programming. This approach reduces the search time and required data amount by orders of magnitude, with little compromise on quantization accuracy. Specifically, on post-training quantization, we achieve 71.27% Top-1 accuracy on MobileNetV2, which only takes 9 seconds for searching and 1.4 GPU hours for finetuning on ImageNet. Our codes are available at <https://github.com/MAC-AutoML/OMPQ>.

1 Introduction

Recently, we witness an obvious trend in deep learning that the models have rapidly increasing complexity (He et al. 2016; Simonyan and Zisserman 2014; Szegedy et al. 2015; Howard et al. 2017; Sandler et al. 2018; Zhang et al. 2018b). But due to practical limits such as latency, battery, and temperature, the host hardware where the models are deployed cannot keep up with this trend. It results in a large and ever increasing gap between the computational demands and resources. To address this issue, network quantization (Courbariaux et al. 2016; Rastegari et al. 2016), which maps single precision floating point weights or activations to lower bits or integers for compression and acceleration, has attracted considerable research attention. Network quantization can be naturally formulated as an integer programming problem and a straightforward approach is to relax the constraints to make it a tractable optimization problem, at a cost of an approximated solution, e.g. Straight Through Estimation (STE) (Bengio, Léonard, and Courville 2013).

With the recent development of inference hardware, arithmetic operations with variable bit-width become a possibil-

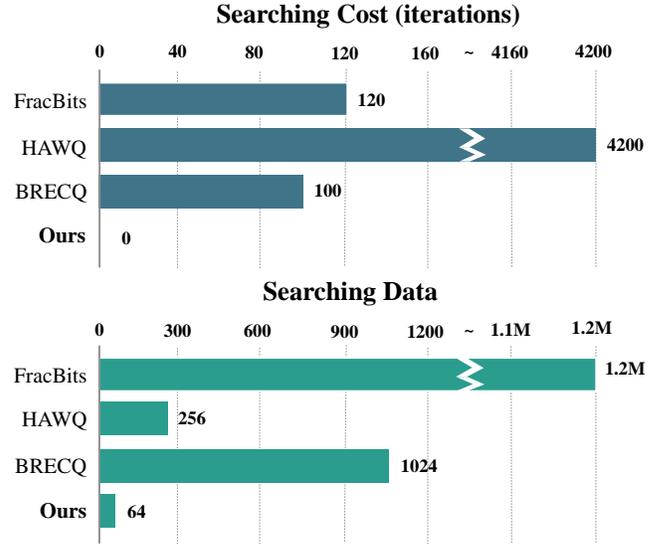


Figure 1: Comparison of the resources used to obtain the optimal bit configuration between our algorithm and other mixed precision algorithms (FracBits (Yang and Jin 2021), HAWQ (Dong et al. 2020), BRECQ (Li et al. 2021)) on ResNet-18. “Searching Data” is the number of input images.

ity, and bring further flexibility to the network quantization. To take full advantage of the hardware capability, mixed precision quantization (Dong et al. 2020; Wang et al. 2019; Li et al. 2021; Yang and Jin 2021) aims to quantize different network layers to different bit configurations, so as to achieve a better trade-off between compression ratio and accuracy compared to traditional unified quantization. While benefiting from the extra flexibility, mixed precision quantization also suffers from a more complicated and challenging optimization problem, with a non-differentiable and extremely non-convex objective function. Therefore, existing approaches (Dong et al. 2020; Yang and Jin 2021; Wang et al. 2019; Li et al. 2021) often require numerous data and computing resources to search for the optimal bit configuration. For instance, FracBits (Yang and Jin 2021) approximates the bit width by performing a first-order Taylor expansion at the adjacent integer, making the variable differentiable. This allows it to integrate search process into training

*Corresponding Author: jintaisong@xmu.edu.cn

to obtain the optimal bit configuration. However, to derive a decent solution, it still requires a large amount of computation resources in the searching and training process. To resolve the large demand on training data, Dong *et al.* (Dong et al. 2020) uses the average eigenvalue of the hessian matrix of each layer as the metric for bit allocation. However, the matrix-free Hutchinson algorithm for implicitly calculating the average of the eigenvalues of the hessian matrix still needs 200 iterations for each network layer. Another direction is black box optimization. For instance, Wang *et al.* (Wang et al. 2019) use reinforcement learning for the bit allocation of each layer. Li *et al.* (Li et al. 2021) use evolutionary search algorithm (Guo et al. 2020) to derive the optimal bit configuration, together with a block reconstruction strategy to efficiently optimize the quantized model, which is called **Post-Training Quantization (PTQ)**. But the population evolution process requires 1,024 input data and 100 iterations, and thus still demands on computation and data.

Different from the existing approaches of black box optimization or constraint relaxation, we propose to construct a proxy metric, which could be substantially different form, but highly correlated with the objective function of the original integer programming. Specifically, we propose an intuitive metric named **OR**thogonality **M**etric (ORM) as the proxy objective. As illustrated in Fig. 1, we only need a single-pass search process on a small amount of data. Specifically, we propose to obtain the optimal bit configuration by using the orthogonality of neural network. According to the research of representation learning (Bengio, Courville, and Vincent 2013), the expressive capability of the model is correlated to its number of parameters. The mixed precision quantization can be viewed as a redistribution of network parameters, so the bit width of each layer is also positively correlated with the expressive capability of the model. Therefore, we deconstruct the neural network model into a set of functions, and define the orthogonality of the model by extending its definition from a function $f : R \rightarrow R$ to the entire network $f : R^m \rightarrow R^n$. The measurement of the orthogonality could be efficiently performed with Monte Carlo sampling and Cauchy-Schwarz inequality, based on which we can then assign a larger bit-width to the layer with larger orthogonality to maximize the layers’ expressive capability and the mutual information during the quantization process. We then further integrate the network orthogonality with specific constraints to construct a linear programming problem to obtain the optimal bit configuration.

In summary, our contributions are listed as follows:

- We introduce a novel metric of layer orthogonality to model the mutual information among layers, and leverage it as a proxy metric to efficiently solve the mixed precision quantization problem, which is the first attempt in the community and can easily be integrated into other quantization frameworks.
- We explore the theoretical properties of the proposed orthogonality and prove that network orthogonality is orthogonal invariant and scale invariant, which demonstrates its robustness.
- We use the orthogonality metric to construct a linear pro-

gramming problem, which can derive the optimal bit-width configuration in a few seconds on a single CPU and GPU. In addition, linear programming allows flexible and variable bit search space.

- We also provide extensive experiments on ImageNet, which demonstrate that the proposed orthogonality based approach could provide state-of-the-art quantization performance with orders of magnitude’s speed up.

2 Related Work

Quantized Neural Networks Existing neural network quantization algorithms can be divided into two categories based on their training strategy: post-training quantization (PTQ) and quantization-aware training (QAT). Post-training quantization (Li et al. 2021; Cai et al. 2020; Nagel et al. 2019) is an offline quantization method, which only needs a small amount of data to complete quantization process. Therefore, PTQ could obtain an optimal quantized model efficiently, at a cost of accuracy drop from quantization. In contrast, quantization-aware training (Dong et al. 2020; Zhou et al. 2017; Chen, Wang, and Pan 2019; Cai et al. 2017; Choi et al. 2018) adopts online quantization strategy. This type of methods utilize the whole training dataset during quantization process. As a result, it has superior accuracy but limited efficiency.

If viewed from a perspective of bit-width allocation granularity, neural network quantization can also be divided into unified and mixed precision quantization. Traditionally, network quantization means unified quantization. Choi *et al.* (Choi et al. 2018) aims to optimize the parameterized clip boundary of activation value of each layer during training process. Chen *et al.* (Chen, Wang, and Pan 2019) introduces the meta-quantization block to approximate the derivative of non-derivable function. Recently, some works (Yang and Jin 2021; Dong et al. 2020; Li et al. 2021) that explore assigning different bit-widths to different layers begin to emerge. We have already introduced these methods in the Sec. 1.

Network Similarity Previous works (Gretton et al. 2005; Kornblith et al. 2019) are also devoted to discovering the correlation between different layers of neural networks. Gretton *et al.* (Gretton et al. 2005) proposed the Hilbert-Schmidt Independence Criterion (HSIC), and gave a finite-dimensional approximation of it. Furthermore, Kornblith *et al.* (Kornblith et al. 2019) propose the similarity criterion CKA based on HSIC, and studies its relationship with other similarity criteria. These works are enlightening and theoretically sound, but are highly complicated and hard to implement. We propose a metric from the perspective of network orthogonality, and give a simple and clear derivation.

3 Methodology

In this section, we will introduce our mixed precision quantization algorithm from three aspects: how to define the orthogonality, how to efficiently measure it, and how to construct a linear programming model to obtain the optimal bit configuration.

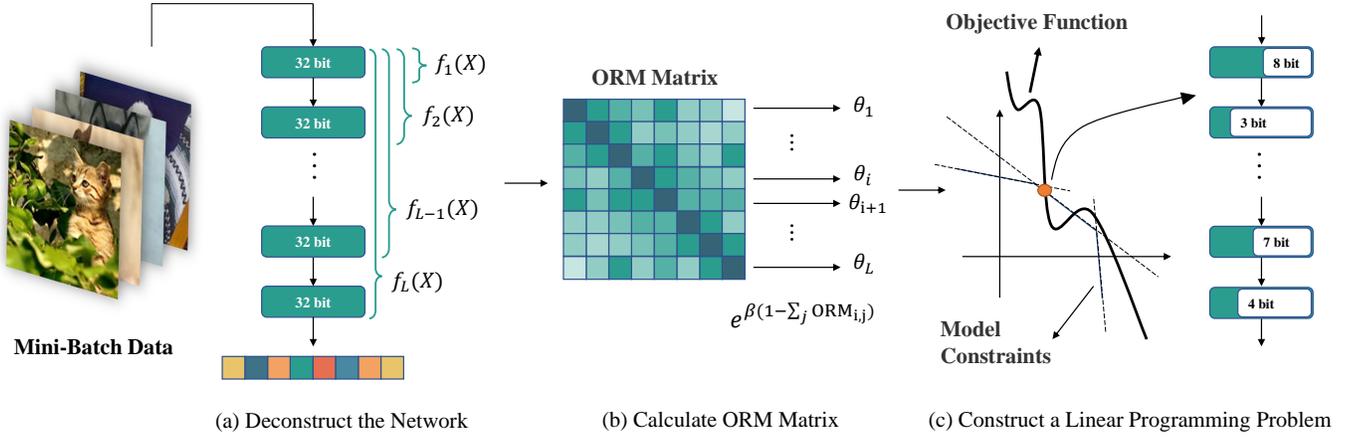


Figure 2: An overview of OMPQ. Left: Deconstruct the model into a set of functions \mathcal{F} . Middle: ORM symmetric matrix calculated from \mathcal{F} . Right: Linear programming problem constructed by the importance factor θ to derive optimal bit configuration.

3.1 Network Orthogonality

A neural network can be naturally decomposed into a set of layers or functions. Formally, for the given input $x \in \mathcal{R}^{1 \times (C \times H \times W)}$, we decompose a neural network into $\mathcal{F} = \{f_1, f_2, \dots, f_L\}$, where f_i represents the transformation from input x to the result of the i -th layer. In other words, if g_i represents the function of the i -th layer, then $f_i(x) = g_i(f_{i-1}(x)) = g_i(g_{i-1}(\dots g_1(x)))$. Here we introduce the inner product (Arfken and Weber 1999) between functions f_i and f_j , which is formally defined as,

$$\langle f_i, f_j \rangle_{P(x)} = \int_{\mathcal{D}} f_i(x) P(x) f_j(x)^T dx, \quad (1)$$

where $f_i(x) \in \mathcal{R}^{1 \times (C_i \times H_i \times W_i)}$, $f_j(x) \in \mathcal{R}^{1 \times (C_j \times H_j \times W_j)}$ are known functions when the model is given, and \mathcal{D} is the domain of x . $P(x) \in \mathcal{R}^{(C_i \times H_i \times W_i) \times (C_j \times H_j \times W_j)}$ is the probability density matrix between $f_i(x)$ and $f_j(x)$. According to the definition (Arfken and Weber 1999), $\langle f_i, f_j \rangle_{P(x)} = 0$ means that f_i and f_j are weighted orthogonal. In other words, $\langle f_i, f_j \rangle_{P(x)}$ is negatively correlated with the orthogonality between f_i and f_j . When we have a known set of functions to be quantized $\mathcal{F} = \{f_i\}_{i=1}^L$, with the goal to approximate an arbitrary function h^* , the quantization error can then be expressed by the mean square error: $\xi \int_{\mathcal{D}} |h^*(x) - \sum_i \psi_i f_i(x)|^2 dx$, where ξ and ψ_i are error coefficient and combination coefficient, respectively. According to Parseval equality (Tanton 2005), if \mathcal{F} is orthogonal basis functions set, then the mean square error could achieve 0. Furthermore, the orthogonality between the basis functions is stronger, the mean square error is smaller, i.e. the model corresponding to the linear combination of basis functions has a stronger expressive capability. Here we further introduce this insight to the network quantization. Specifically, we propose to assign a larger bit width to the layer with stronger orthogonality against all other layers to maximize the expressive capability of the model. However, Eq. 1 has the integral of a continuous function which is untractable in

practice. Therefore, we derive a new metric to efficiently approximate the orthogonality of each layer in Sec. 3.2

3.2 Efficient Orthogonality Metric

We propose to leverage the Monte Carlo sampling to approximate the orthogonality of the layers, to avoid the intractable integral. Specifically, from a Monte Carlo sampling perspective, Eq. 1 can be rewritten as

$$\begin{aligned} \langle f_i, f_j \rangle_{P(x)} &= \int_{\mathcal{D}} f_i(x) P(x) f_j(x)^T dx \\ &= \left\| E_{P(x)}[f_j(x)^T f_i(x)] \right\|_F. \end{aligned} \quad (2)$$

We randomly get N samples x_1, x_2, \dots, x_N from a training dataset with the probability density matrix $P(x)$, which allows the expectation $E_{P(x)}[f_j(x)^T f_i(x)]$ to be further approximated as,

$$\begin{aligned} \left\| E_{P(x)}[f_j(x)^T f_i(x)] \right\|_F &\approx \frac{1}{N} \left\| \sum_{n=1}^N f_j(x_n)^T f_i(x_n) \right\|_F \\ &= \frac{1}{N} \|f_j(X)^T f_i(X)\|_F, \end{aligned} \quad (3)$$

where $f_i(X) \in \mathcal{R}^{N \times (C_i \times H_i \times W_i)}$ represents the output of the i -th layer, $f_j(X) \in \mathcal{R}^{N \times (C_j \times H_j \times W_j)}$ represents the output of the j -th layer, and $\|\cdot\|_F$ is the Frobenius norm. From Eqs. 2 and 3, we have,

$$N \int_{\mathcal{D}} f_i(x) P(x) f_j(x)^T dx \approx \|f_j(X)^T f_i(X)\|_F. \quad (4)$$

However, the comparison of orthogonality between different layers is difficult due to the differences in dimensionality. To this end, we use the Cauchy-Schwarz inequality to normalize it in $[0, 1]$ for different layers. Applying Cauchy-Schwarz inequality to the left side of Eq. 4, we can get

$$\begin{aligned}
0 &\leq \left(N \int_{\mathcal{D}} f_i(x) P(x) f_j(x)^T dx \right)^2 \\
&\leq \int_{\mathcal{D}} N f_i(x) P_i(x) f_i(x)^T dx \int_{\mathcal{D}} N f_j(x) P_j(x) f_j(x)^T dx.
\end{aligned} \tag{5}$$

We substitute Eq. 4 into Eq. 5 and perform some simplifications to derive our **OR**thogonality **M**etric (ORM):

$$\text{ORM}(X, f_i, f_j) = \frac{\|f_j(X)^T f_i(X)\|_F^2}{\|f_i(X)^T f_i(X)\|_F \|f_j(X)^T f_j(X)\|_F}, \tag{6}$$

where $\text{ORM} \in [0, 1]$. f_i and f_j is orthogonal when $\text{ORM} = 0$. On the contrary, f_i and f_j is dependent when $\text{ORM} = 1$. Therefore, ORM is negatively correlated to orthogonality. In addition, ORM is invariant to orthogonal transformation Q and scale transformation α , which shows that ORM is more stable and robust than other independence criteria (Morcos, Raghu, and Bengio 2018; Kornblith et al. 2019). Specifically, ORM satisfies

$$\begin{aligned}
&\text{ORM}(X, Qf_i, f_j) \\
&= \frac{\|f_j(X)^T Qf_i(X)\|_F^2}{\|f_i(X)^T Qf_i(X)\|_F \|f_j(X)^T f_j(X)\|_F} \\
&= \text{ORM}(X, f_i, f_j),
\end{aligned} \tag{7}$$

which indicates that ORM is invariant to orthogonal transformations. Meanwhile, ORM also satisfies

$$\begin{aligned}
&\text{ORM}(X, \alpha f_i, f_j) \\
&= \frac{\|f_j(X)^T \alpha f_i(X)\|_F^2}{\|\alpha f_i(X)^T \alpha f_i(X)\|_F \|f_j(X)^T f_j(X)\|_F} \\
&= \text{ORM}(X, f_i, f_j),
\end{aligned} \tag{8}$$

which indicates the invariance of scale transformation. Orthogonal transformation breaks the permutation symmetry of a network and eliminates the singularity of network units (Orhan and Pitkow 2018). And scale transformation which exists widely in the BatchNorm layer (Ioffe and Szegedy 2015) greatly impact the network presentation. Therefore, the orthogonal invariance and scale invariance of ORM are necessary. The detailed proofs of Eqs. 7 and 8 are provided in the supplementary material. Besides, we also provide experiment comparison on the scale invariance and orthogonality invariance between ORM and other independence criteria, the results are reported in Sec. 4.2.

3.3 Mixed Precision Quantization

For a specific neural network, we can calculate an orthogonality matrix K , where $k_{ij} = \text{ORM}(X, f_i, f_j)$. Obviously, K is a symmetric matrix and the diagonal elements are 1. We add up the non-diagonal elements of each row of the matrix,

$$\gamma_i = \sum_{j=1}^L k_{ij} - 1. \tag{9}$$

Algorithm 1: OMPQ

Input: Pre-trained model M with L layers, small batch of data X sampled independently and identically.

Output: Optimal bit allocation \mathbf{b} of the model.

- 1: Input X to M and derive function set $\mathcal{F} = \{f_1, \dots, f_L\}$;
 - 2: **for** $f_i = f_1, \dots, f_L$ **do**
 - 3: **for** $f_j = f_1, \dots, f_L$ **do**
 - 4: Calculate $k_{i,j} = \text{ORM}(X, f_i, f_j)$ by Eq. 6;
 - 5: **end for**
 - 6: **end for**
 - 7: Calculate layer orthogonality γ_i by Eq. 9;
 - 8: Calculate importance factor θ_i by Eq. 10;
 - 9: Solve the linear programming problem as Eq. 11;
 - 10: **return** \mathbf{b} .
-

The smaller the γ_i means the stronger the orthogonality between f_i and other functions in the function set \mathcal{F} , and it also means that former i layers of the neural network is more independent. Thus, we leverage the monotonically decreasing function e^{-x} to model this relationship:

$$\theta_i = e^{-\beta \gamma_i}, \tag{10}$$

where β is a hyper-parameter to control the bit width difference between different layers. We also investigate some other monotonically decreasing functions (For the details, please refer to Sec. 4.2). θ_i is used as the importance factor for the former i layers of the network, then we define a linear programming problem as follows:

$$\begin{aligned}
&\text{Objective: } \max_{\mathbf{b}} \sum_{i=1}^L \left(\frac{b_i}{L-i+1} \sum_{j=i}^L \theta_j \right), \\
&\text{Constraints: } \sum_i^L M^{(b_i)} \leq \mathcal{T}.
\end{aligned} \tag{11}$$

$M^{(b_i)}$ is the model size of the i -th layer under b_i bit quantization and \mathcal{T} represents the target model size. Maximizing the objective function means assigning a larger bit width to the more independent layer, which implicitly maximizes the model's representation capability.

Note that it is extremely efficient to solve the linear programming problem in Eq. 11, which only takes a few seconds on a single CPU. In other words, our method is extremely effective (9s on MobileNetV2) when comparing to the previous methods (Yang and Jin 2021; Dong et al. 2020; Li et al. 2021) that requires lots of data or iterations for searching. In addition, our algorithm can be used as a plug-and-play module to combine with quantization-aware training or post-training quantization methods thanks to the high efficiency and low data requirements. In other words, our approach is capable of improving accuracy of SOTA methods, where experiment results are reported in Sec. 4.3 and 4.4. The proposed algorithm is summarized in Alg. 1.

3.4 Calculation Acceleration

Given a specific model, the dimension of features is increasing with the layer. Thus, calculating Eq. 6 involves huge matrices. In the following, we analyze the computation complexity of the ORM between f_i and f_j . Suppose that $f_i(X) \in \mathcal{R}^{N \times (C_i \times H_i \times W_i)}$, $f_j(X) \in \mathcal{R}^{N \times (C_j \times H_j \times W_j)}$, and dimension of features in the j -th layer is larger than the i -th layer. Furthermore, the time complexity of computing $\text{ORM}(X, f_i, f_j)$ is $\mathcal{O}(NC_j^2 H_j^2 W_j^2)$. The huge matrix occupies a lot of memory resources, and also increases the time complexity of the entire algorithm by several orders of magnitude. Therefore, we derive an equivalent form to accelerate calculation. If we take $Y = f_i(X)$, $Z = f_j(X)$ as an example, then $YY^T, ZZ^T \in \mathcal{R}^{N \times N}$. We have:

$$\|Z^T Y\|_F^2 = \langle \text{vec}(YY^T), \text{vec}(ZZ^T) \rangle, \quad (12)$$

where $\text{vec}(\cdot)$ represents the operation of flattening the matrix into a vector. From Eq. 13, we can observe that calculating the Frobenius norm of a matrix is transformed into the inner product of vectors, and the time complexity of calculating $\text{ORM}(X, f_i, f_j)$ becomes $\mathcal{O}(N^2 C_j H_j W_j)$. When the samples N is larger than the dimension of features $C \times H \times W$, the norm form is faster to calculate thanks to lower time complexity and vice versa. We have demonstrated the specific acceleration ratio and the proof of Eq. 13 in supplementary material. Specifically, when the dimension of the features is larger than the samples, the average acceleration ratio can reach about 70x.

4 Experiments

In this section, we conduct a series of experiments to validate the effectiveness of OMPQ on ImageNet. We first introduce the implementation details of our experiments. And then, ablation experiments about the invariance of ORM, monotonically decreasing function, and deconstruction granularity are conducted to demonstrate the importance of each component. Finally, we combine OMPQ with widely-used QAT and PTQ methods, which shows a better compression and accuracy trade-off comparing to the SOTA methods.

4.1 Implementation Details

The ImageNet dataset includes 1.2M training data and 50,000 validation data. We randomly obtain 64 training data for ResNet-18/50 and 32 training data for MobileNetV2 following similar data pre-processing (He et al. 2016) to get the set of functions \mathcal{F} . OMPQ is extremely effective which only needs a piece of Nvidia Geforce GTX 1080Ti and a single Intel(R) Xeon(R) CPU E5-2620 v4. For the models that have a large amount of parameters, we directly adopt round function to convert the bit-width into an integer after linear programming. Meanwhile, we adopt depth-first search (DFS) to find the bit configuration that strictly meets the different constraints for small model, e.g. ResNet-18. The aforementioned processes are extremely effective, which only take a few seconds on these devices. Besides, OMPQ is flexible, which is capable of leveraging different search spaces with QAT and PTQ under different requirements. Finetuning implementation details are listed in supplementary material.

4.2 Ablation Study

Invariance. We compare the scale invariance and orthogonality invariance of ORM to projection-weighted canonical correlation (PWCCA) (Morcos, Raghu, and Bengio 2018) and Linear Hilbert-Schmidt Independence Criterion (Linear HSIC) (Kornblith et al. 2019). In order to check the scale and orthogonal invariance, we randomly generate $X, Y \in \mathcal{R}^{100 \times 10}$, orthogonal matrix $Q \in \mathcal{R}^{10 \times 10}$, and take scale $\alpha = 1.5$. Then, we perform orthogonal transformation QX and scale transformation αX . Finally, we calculate absolute difference of the criterion before and after the transformation. The results are listed in Tab. 1. It can be seen that PWCCA does not have orthogonal invariance, and Linear HSIC is sensitive to scale transformation. Meanwhile, ORM is more stable and robust to perturbation than other criteria.

Independence Criterion	Orthogonal Transformation	Scale Transformation
PWCCA	0.02	0
Linear HSIC	0	15.42
ORM	0	0

Table 1: Comparison of independence criterion on orthogonal invariance and scale invariance. The result is represented as the absolute difference of the criterion before and after the transformation.

Monotonically Decreasing Function. We then investigate the monotonically decreasing function in Eq. 10. Obviously, second-order derivatives of monotonically decreasing functions in Eq. 10 influence the changing rate of orthogonality differences. In other words, the variance of the orthogonality between different layers becomes larger as the rate becomes faster. We tested the accuracy of five different monotonically decreasing functions on quantization-aware training of ResNet-18 (6.7Mb) and post-training quantization of MobileNetV2 (0.9Mb). We fix the activation to 8 bit.

Decreasing Function	ResNet-18 (%)	MobileNetV2 (%)	Changing Rate
e^{-x}	72.30	63.51	e^{-x}
$-\log x$	72.26	63.20	x^{-2}
$-x$	72.36	63.0	0
$-x^3$	71.71	-	$6x$
$-e^x$	-	-	e^x

Table 2: The Top-1 accuracy (%) with different monotonically decreasing functions on ResNet-18 and MobileNetV2.

It can be observed from Tab. 2 that the accuracy gradually decreases with the increasing of changing rate. In the corresponding bit configuration, we also observe that a larger changing rate also means a more aggressive bit allocation strategy. In other words, OMPQ tends to assign more different bits under a large changing rate, which leads to a worse performance in network quantization. Another interesting observation is the accuracy on ResNet-18 and MobileNetV2.

(a) ResNet-18

Method	W bit	A bit	Int-Only	Uniform	Model Size (Mb)	BOPs (G)	Top-1 (%)
Baseline	32	32	✗	-	44.6	1,858	73.09
RVQuant	8	8	✗	✗	11.1	116	70.01
HAWQ-V3	8	8	✓	✓	11.1	116	71.56
OMPQ	mixed	8	✓	✓	6.7	97	72.30
PACT	5	5	✗	✓	7.2	74	69.80
LQ_Nets	4	32	✗	✗	5.8	225	70.00
HAWQ-V3	mixed	mixed	✓	✓	6.7	72	70.22
OMPQ	mixed	6	✓	✓	6.7	75	72.08

(b) ResNet-50

Method	W bit	A bit	Int-Only	Uniform	Model Size (Mb)	BOPs (G)	Top-1 (%)
Baseline	32	32	✗	-	97.8	3,951	77.72
PACT	5	5	✗	✓	16.0	133	76.70
LQ_Nets	4	32	✗	✗	13.1	486	76.40
RVQuant	5	5	✗	✗	16.0	101	75.60
HAQ	mixed	32	✗	✗	9.62	520	75.48
OneBitwidth	mixed	8	✗	✓	12.3	494	76.70
HAWQ-V3	mixed	mixed	✓	✓	18.7	154	75.39
OMPQ	mixed	5	✓	✓	16.0	141	76.20
OMPQ	mixed	5	✓	✓	18.7	156	76.28

Table 3: Mixed precision quantization results of ResNet-18 and ResNet-50. ‘‘Int-Only’’ means only including integer during quantization process. ‘‘Uniform’’ represents uniform quantization.

Model	W bit	Layer	Block	Stage	Net
ResNet-18	5*	72.51	72.52	72.47	72.31
MobileNetV2	3*	69.37	69.10	68.86	63.99

Table 4: Top-1 accuracy (%) of different deconstruction granularity. The activations are both quantized to 8 bit.

Specifically, quantization-aware training on ResNet-18 requires numerous data, which makes the change of accuracy insignificant. On the contrary, post-training quantization on MobileNetV2 is incapable of assigning bit configuration that meets the model constraints when the functions are set to $-x^3$ or $-e^x$. To this end, we select e^{-x} as our monotonically decreasing function in the following experiments.

Deconstruction Granularity. We study the impact of different deconstruction granularity on model accuracy. Specifically, we test four different granularity including layer-wise, block-wise, stage-wise and net-wise on the quantized-aware training of ResNet-18 and the post-training quantization of MobileNetV2. As reported in Tab. 4, the accuracy of the two models is increasing with finer granularities. Such difference is more significant in MobileNetV2 due to the sensitiveness

of the depth-wise convolution. We thus employ layer-wise granularity in our following experiments.

4.3 Quantization-Aware Training

We first perform quantization-aware training on ResNet-18/50, where the results and compress ratio are compared with the previous unified quantization methods (Park, Yoo, and Vajda 2018; Choi et al. 2018; Zhang et al. 2018a) and mixed precision quantization (Wang et al. 2019; Chin et al. 2020; Yao et al. 2021). As shown in Tab. 3, OMPQ shows the best trade-off between accuracy and compress ratio on ResNet-18/50. For example, we achieve 72.08% on ResNet-18 with only 6.7Mb and 75BOPs. Comparing with HAWQ-V3(Yao et al. 2021), the difference of the model size are negligible (6.7Mb, 75BOPs vs 6.7Mb, 72BOPs). Meanwhile, the model compressed by OMPQ is 1.86% higher than HAWQ-V3(Yao et al. 2021). Similarly, we achieve 76.28% on ResNet-50 with 18.7Mb and 156BOPs. And OMPQ is 0.89% higher than HAWQ-V3 with similar model size (18.7Mb, 156BOPs vs 18.7Mb, 154BOPs).

4.4 Post-Training Quantization

As we mentioned before, OMPQ can also be combined with PTQ to further improve the quantization efficiency thanking

(a) ResNet-18

Method	W bit	A bit	Model Size (Mb)	Top-1 (%)	Searching Data	Searching Iterations
Baseline	32	32	44.6	71.08	-	-
FracBits-PACT	mixed	mixed	4.5	69.10	1.2M	120
OMPQ+BRECQ	mixed	4	4.5	68.69	64	0
OMPQ+BRECQ	mixed	8	4.5	69.73	64	0
ZeroQ	4	4	5.81	21.20	-	-
BRECQ (W/ Distilled Data)	4	4	5.81	69.32	-	-
PACT	4	4	5.81	69.20	-	-
HAWQ-V3	4	4	5.81	68.45	-	-
FracBits-PACT	mixed	mixed	5.81	69.70	1.2M	120
OMPQ+BRECQ	mixed	4	5.5	69.38	64	0
BRECQ	mixed	8	4.0	68.82	1,024	100
OMPQ+BRECQ	mixed	8	4.0	69.34	64	0

(b) MobileNetV2

Method	W bit	A bit	Model Size (Mb)	Top-1 (%)	Searching Data	Searching Iterations
Baseline	32	32	13.4	72.49	-	-
BRECQ	mixed	8	1.3	68.99	1,024	100
OMPQ+BRECQ	mixed	8	1.3	69.51	32	0
FracBits	mixed	mixed	1.84	69.90	1.2M	120
BRECQ	mixed	8	1.5	70.28	1,024	100
OMPQ+BRECQ	mixed	8	1.5	71.27	32	0

Table 5: Mixed precision post-training quantization experiments on ResNet-18 and MobileNetV2.

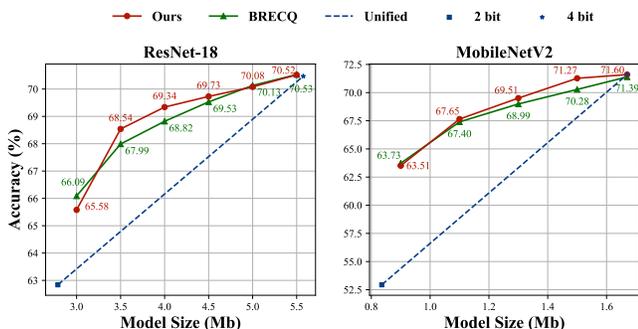


Figure 3: Mixed precision quantization comparison of OMPQ and BRECQ on ResNet-18 and MobileNetV2.

to its low data dependence and search efficiency. Previous PTQ method BRECQ (Li et al. 2021) proposes block reconstruction quantization strategy to reduce quantization errors. We integrate the finetuning process of BRECQ into OMPQ, where the search cost is rapidly reduced and achieves the better performance. Experiment results are demonstrated in Tab. 5, we can observe that the OMPQ clearly shows a superior performance to a large number of unified quantization and mixed precision quantization methods under different model constraints. In particular, OMPQ outperforms BRECQ by 0.52% on ResNet-18 under the same model size

(4.0Mb). OMPQ also outperforms FracBits by 1.37% on MobileNetV2 with a smaller model size (1.5Mb vs 1.8Mb).

We also compare OMPQ with BRECQ and unified quantization, where the results are reported in Fig. 3. Obviously, the accuracy of OMPQ is generally higher than BRECQ on ResNet-18 and MobileNetV2 with different model constraints. Furthermore, OMPQ and BRECQ are better than unified quantization, which shows that mixed precision quantization is superior.

5 Conclusion

In this paper, we have proposed a novel mixed precision algorithm, termed OMPQ, to effectively search the optimal bit configuration on the different constraints. Firstly, we derive the orthogonality metric of neural network by generalizing the orthogonality of the function to the neural network. Secondly, we leverage the proposed orthogonality metric to design a linear programming problem, which is capable of finding the optimal bit configuration. Both orthogonality generation and linear programming solving are extremely effective, which are finished within a few seconds on a single CPU and GPU. Meanwhile, OMPQ also outperforms the previous mixed precision quantization and unified quantization methods. For future work, we will study the mixed precision quantization method combining the multiple knapsack problem with the network orthogonality metric.

References

- Arfken, G. B.; and Weber, H. J. 1999. *Mathematical Methods for Physicists*.
- Bengio, Y.; Courville, A.; and Vincent, P. 2013. Representation Learning: A Review and New Perspectives. *IEEE Transactions on Pattern Analysis and Machine Intelligence (TPAMI)*, 35: 1798–1828.
- Bengio, Y.; Léonard, N.; and Courville, A. 2013. Estimating or Propagating Gradients through Stochastic Neurons for Conditional Computation. *arXiv preprint arXiv:1308.3432*.
- Cai, Y.; Yao, Z.; Dong, Z.; Gholami, A.; Mahoney, M. W.; and Keutzer, K. 2020. Zeroq: A Novel Zero Shot Quantization Framework. In *Computer Vision and Pattern Recognition (CVPR)*, 13169–13178.
- Cai, Z.; He, X.; Sun, J.; and Vasconcelos, N. 2017. Deep Learning with Low Precision by Half-Wave Gaussian Quantization. In *Computer Vision and Pattern Recognition (CVPR)*, 5918–5926.
- Chen, S.; Wang, W.; and Pan, S. J. 2019. Metaquant: Learning to Quantize by Learning to Penetrate Non-Differentiable Quantization. *Neural Information Processing Systems (NeurIPS)*, 32: 3916–3926.
- Chin, T.-W.; Pierce, I.; Chuang, J.; Chandra, V.; and Marculescu, D. 2020. One Weight Bitwidth to Rule Them All. In *European Conference on Computer Vision (ECCV)*, 85–103.
- Choi, J.; Wang, Z.; Venkataramani, S.; Chuang, P. I.-J.; Srinivasan, V.; and Gopalakrishnan, K. 2018. Pact: Parameterized Clipping Activation for Quantized Neural Networks. *arXiv preprint arXiv:1805.06085*.
- Courbariaux, M.; Hubara, I.; Soudry, D.; El-Yaniv, R.; and Bengio, Y. 2016. Binarized Neural Networks: Training Deep Neural Networks with Weights and Activations constrained to +1 or -1. *arXiv preprint arXiv:1602.02830*.
- Dong, Z.; Yao, Z.; Arfeen, D.; Gholami, A.; Mahoney, M. W.; and Keutzer, K. 2020. HAWQ-V2: Hessian Aware Trace-Weighted Quantization of Neural Networks. In *Neural Information Processing Systems (NeurIPS)*, 18518–18529.
- Gretton, A.; Bousquet, O.; Smola, A.; and Schölkopf, B. 2005. Measuring Statistical Dependence with Hilbert-Schmidt Norms. In *Algorithmic Learning Theory (ALT)*, 63–77.
- Guo, Z.; Zhang, X.; Mu, H.; Heng, W.; Liu, Z.; Wei, Y.; and Sun, J. 2020. Single Path One-Shot Neural Architecture Search with Uniform Sampling. In *European Conference on Computer Vision (ECCV)*, 544–560.
- He, K.; Zhang, X.; Ren, S.; and Sun, J. 2016. Deep Residual Learning for Image Recognition. In *Computer Vision and Pattern Recognition (CVPR)*, 770–778.
- Howard, A. G.; Zhu, M.; Chen, B.; Kalenichenko, D.; Wang, W.; Weyand, T.; Andreetto, M.; and Adam, H. 2017. Mobilenets: Efficient Convolutional Neural Networks for Mobile Vision Applications. *arXiv preprint arXiv:1704.04861*.
- Ioffe, S.; and Szegedy, C. 2015. Batch Normalization: Accelerating Deep Network Training by Reducing Internal Covariate Shift. In *International Conference on Machine Learning (ICML)*, 448–456.
- Kornblith, S.; Norouzi, M.; Lee, H.; and Hinton, G. 2019. Similarity of Neural Network Representations Revisited. In *International Conference on Machine Learning (ICML)*, 3519–3529.
- Li, Y.; Gong, R.; Tan, X.; Yang, Y.; Hu, P.; Zhang, Q.; Yu, F.; Wang, W.; and Gu, S. 2021. {BRECQ}: Pushing the Limit of Post-Training Quantization by Block Reconstruction. In *International Conference on Learning Representations (ICLR)*.
- Morcos, A. S.; Raghu, M.; and Bengio, S. 2018. Insights on Representational Similarity in Neural Networks with Canonical Correlation. In *Neural Information Processing Systems (NeurIPS)*, 5732–5741.
- Nagel, M.; Baalen, M. v.; Blankevoort, T.; and Welling, M. 2019. Data-Free Quantization through Weight Equalization and Bias Correction. In *International Conference on Computer Vision (ICCV)*, 1325–1334.
- Orhan, E.; and Pitkow, X. 2018. Skip Connections Eliminate Singularities. In *International Conference on Learning Representations (ICLR)*.
- Park, E.; Yoo, S.; and Vajda, P. 2018. Value-Aware Quantization for Training and Inference of Neural Networks. In *European Conference on Computer Vision (ECCV)*, 580–595.
- Rastegari, M.; Ordonez, V.; Redmon, J.; and Farhadi, A. 2016. Xnor-net: Imagenet Classification Using Binary Convolutional Neural Networks. In *European Conference on Computer Vision (ECCV)*, 525–542.
- Sandler, M.; Howard, A.; Zhu, M.; Zhmoginov, A.; and Chen, L.-C. 2018. Mobilenetv2: Inverted Residuals and Linear Bottlenecks. In *Computer Vision and Pattern Recognition (CVPR)*, 4510–4520.
- Simonyan, K.; and Zisserman, A. 2014. Very Deep Convolutional Networks for Large-Scale Image Recognition. *arXiv preprint arXiv:1409.1556*.
- Szegedy, C.; Liu, W.; Jia, Y.; Sermanet, P.; Reed, S.; Anguelov, D.; Erhan, D.; Vanhoucke, V.; and Rabinovich, A. 2015. Going Deeper with Convolutions. In *Computer Vision and Pattern Recognition (CVPR)*, 1–9.
- Tanton, J. 2005. *Encyclopedia of Mathematics*. Facts on file.
- Wang, K.; Liu, Z.; Lin, Y.; Lin, J.; and Han, S. 2019. Haq: Hardware-Aware Automated Quantization with Mixed Precision. In *Computer Vision and Pattern Recognition (CVPR)*, 8612–8620.
- Yang, L.; and Jin, Q. 2021. FracBits: Mixed Precision Quantization via Fractional Bit-Widths. *AAAI Conference on Artificial Intelligence (AAAI)*, 35: 10612–10620.
- Yao, Z.; Dong, Z.; Zheng, Z.; Gholami, A.; Yu, J.; Tan, E.; Wang, L.; Huang, Q.; Wang, Y.; Mahoney, M.; et al. 2021. HAWQ-V3: Dyadic Neural Network Quantization. In *International Conference on Machine Learning (ICML)*, 11875–11886.

Zhang, D.; Yang, J.; Ye, D.; and Hua, G. 2018a. Lq-nets: Learned Quantization for Highly Accurate and Compact Deep Neural Networks. In *European Conference on Computer Vision (ECCV)*, 365–382.

Zhang, X.; Zhou, X.; Lin, M.; and Sun, J. 2018b. Shufflenet: An Extremely Efficient Convolutional Neural Network for Mobile Devices. In *Computer Vision and Pattern Recognition (CVPR)*, 6848–6856.

Zhou, A.; Yao, A.; Guo, Y.; Xu, L.; and Chen, Y. 2017. Incremental Network Quantization: Towards Lossless CNNs with Low-Precision Weights. In *International Conference on Learning Representations (ICLR)*.

Supplementary Material

Calculation Acceleration

Suppose that $f_i(X) \in \mathcal{R}^{N \times (C_i \times H_i \times W_i)}$ and $f_j(X) \in \mathcal{R}^{N \times (C_j \times H_j \times W_j)}$ are the output of the i -th layer and the j -th layer in the neural network, respectively. We set $Y = f_i(X)$, $Z = f_j(X)$, then $YY^T, ZZ^T \in \mathcal{R}^{N \times N}$. We can get:

$$\|Z^T Y\|_F^2 = \langle \text{vec}(YY^T), \text{vec}(ZZ^T) \rangle. \quad (13)$$

Proof. We set $p_1 = C_i \times H_i \times W_i, p_2 = C_j \times H_j \times W_j$, and $z_{i,m}, y_{i,m}$ are the i -th row and m -th column entry of the matrix Z and Y , then

$$\begin{aligned} & \|Z^T Y\|_F^2 \\ &= \sum_{i=1}^{p_2} \sum_{j=1}^{p_1} \left(\sum_{m=1}^N z_{m,i} y_{m,j} \right)^2 \\ &= \sum_{i=1}^{p_2} \sum_{j=1}^{p_1} \left(\sum_{m=1}^N z_{m,i} y_{m,j} \right) \left(\sum_{n=1}^N z_{n,i} y_{n,j} \right) \\ &= \sum_{i=1}^{p_2} \sum_{j=1}^{p_1} \sum_{m=1}^N \sum_{n=1}^N z_{m,i} y_{m,j} z_{n,i} y_{n,j} \\ &= \sum_{m=1}^N \sum_{n=1}^N \sum_{i=1}^{p_2} \sum_{j=1}^{p_1} z_{m,i} y_{m,j} z_{n,i} y_{n,j} \\ &= \sum_{m=1}^N \sum_{n=1}^N \left(\sum_{j=1}^{p_1} y_{m,j} y_{n,j} \right) \left(\sum_{i=1}^{p_2} z_{m,i} z_{n,i} \right) \\ &= \langle \text{vec}(YY^T), \text{vec}(ZZ^T) \rangle. \end{aligned}$$

□

From Eq. 13, we can obviously notice that two computation forms have different time complexities to deal with different situations. The time complexities of calculating $\|Z^T Y\|_F^2$ and inner product of vectors are $\mathcal{O}(Np_1p_2)$ and $\mathcal{O}(N^2(p_1 + p_2 + 1))$, respectively. If feature number (p_1, p_2) is larger than samples (N), we take the inner product form to speed up the calculation and vice versa.

To give a concrete example, we take $N, p \in \{10000, 100\}$, randomly generate matrix $Y, Z \in \mathcal{R}^{N \times p}$, and we determine the ORM calculation time of matrix Y, Z in vector inner product form and norm form, As shown in Tab. 6, when the number of features is less than the number of samples, calculating ORM in the norm form is much faster ($54 \times$) than the inner product form. On the contrary, when the number of features is greater than the number of samples, the inner product form calculates the ORM faster ($70 \times$).

Invariance

Due to the homogeneity of the Frobenius norm, we can easily derive the scale invariance of the ORM, so we omit its proof. To give the proof of orthogonal invariance, We first introduce a lemma.

	Calculation strategy		Acceleration Ratio
	Inner Product	Norm	
$N > p$	18.42	0.34	$54 \times$
$N < p$	0.12	8.40	$70 \times$

Table 6: The calculation time (second) of the different calculation strategy of the ORM between the matrix Y and Z in the case of different sizes of feature numbers p and samples numbers N .

Lemma 1. Given matrix $Y \in \mathcal{R}^{N \times p_1}, Z \in \mathcal{R}^{N \times p_2}$, we have

$$\|Z^T Y\|_F^2 = \text{tr}(YY^T ZZ^T). \quad (14)$$

Proof.

$$\begin{aligned} & \text{tr}(YY^T ZZ^T) \\ &= \sum_{m=1}^N \sum_{n=1}^N \left(\sum_{j=1}^{p_1} y_{m,j} y_{n,j} \right) \left(\sum_{i=1}^{p_2} z_{m,i} z_{n,i} \right) \\ &= \langle \text{vec}(YY^T), \text{vec}(ZZ^T) \rangle \\ &= \|Z^T Y\|_F^2. \end{aligned}$$

□

Therefore, if Q is the orthogonal matrix, we perform orthogonality transformation QY . Then we prove the orthogonality invariance of the ORM as follows,

Proof.

$$\begin{aligned} & \text{ORM}(X, QY, Z) \\ &= \frac{\|Z^T QY\|_F^2}{\|Y^T Q^T QY\|_F \|Z^T Z\|_F} \\ &= \frac{\text{tr}(QY Y^T Q^T Z Z^T)}{\|Y^T Y\|_F \|Z^T Z\|_F} \\ &= \frac{\text{tr}(Y Y^T Q Q^T Z Z^T)}{\|Y^T Y\|_F \|Z^T Z\|_F} \\ &= \frac{\text{tr}(Y Y^T Z Z^T)}{\|Y^T Y\|_F \|Z^T Z\|_F} \\ &= \text{ORM}(X, Y, Z). \end{aligned}$$

□

Implementation Details

For experiments that is combined with QAT. We use two NVIDIA Tesla V100 GPUs and the implementation is based on HAWQ-V3 (Yao et al. 2021). This method does not exist integer division or floating point numbers in the network. We thus fuse the batch normalization (Ioffe and Szegedy 2015) layer into the convolution layer during the training process. In the training process, initial learning rate is set to $1e-4$, and the batch size is set to 128. We use cosine learning rate scheduler and SGD optimizer with $1e-4$ weight decay during

